*Progress In Electromagnetics Research C, Vol. 137, 17–27, 2023*

# Phase Difference Detection Method for Frequency Tracking in the WPT Systems Using ICST

**Jiliang Yi[1, 2], Shunli Xie[1, *], and Zhongqi Li[1]**

**Abstract**—Wireless Power Transfer (WPT) technology can achieve non-contact transmission of electrical energy from the power grid or batteries to electrical equipment. To solve the problem of a significant decrease in output power caused by frequency detuning in a magnetic coupled resonant WPT system, it is necessary to dynamically adjust the operating frequency of the system. The frequency tracking control tuning using phase locked loop technology is currently the most commonly used method. A new method using incomplete cross S transform (ICST) for phase difference detection is proposed in this paper. Firstly, the low-pass filter is used to eliminate the noise of the original signals, and the waveform of the original voltage signal is changed from pulsed square wave to sinusoidal wave. Then the signals output by the filter are sampled synchronously to obtain a series of discrete signal sequences, and the sampling frequency varies with the operating frequency and is determined by the PI controller. Finally, the phase vector is obtained by performing ICST on two channel discrete signal sequences, and the phase difference, which is provided for subsequent frequency tracking controller between the primary voltage and the primary current, is extracted from the phase vector. The computational complexity of S transformation is greatly reduced by utilizing incomplete S transformation. The effectiveness of the proposed method is verified by MATLAB simulation experiments. Several experiments were conducted separately. The accuracy, noise immunity, and real-time performance of this method are verified under different working conditions.

## 1. INTRODUCTION

Wireless power transmission (WPT) technology can directly transfer electric energy to the load without physical contact, so compared with traditional electric energy transmission it has advantages in terms of convenience, safety, reliability, and flexibility. The transmission distance of magnetic coupling resonant wireless power transmission (MCR-WPT) technology can be from dozens of centimeters to several meters; the transmission power can be from dozens of watts to several kilowatts; and power transfer efficiency is 40% $\sim$ 90%. Due to its obvious advantages in all aspects, it has become the most popular research direction in the current field of WPT [1–4].

In order to achieve the goal of high efficiency and stable operation of the MCR-WPT system, the system must work in resonant state [5]. However, due to changes in load conditions and external environment, as well as the offset of the relative positions of the transmitting and receiving coils, the system is often in a frequency detuning state, resulting in the system being unable to operate at the optimal power and efficiency points [6]. Therefore, it is important to continuously adjust the operating frequency of the WPT system to maintain it in a resonant state [7, 8].

By utilizing frequency tracking control technology, the system can be always operated in a resonant state. System frequency tracking control is a control method that maintains the system in a resonant

*Received 24 May 2023, Accepted 10 August 2023, Scheduled 25 August 2023*
* Corresponding author: Shunli Xie (756691902@qq.com).
[1] College of Railway Transportation, Hunan University of Technology, Zhuzhou 412007, China. [2] School of Automobile Engineering, Guilin University of Aerospace Technology, Guilin 541004, China.

state by controlling the inverter link in real-time, so that the output frequency of the inverter always adapts to the changing system parameters [9, 10]. The most commonly used frequency tracking technology is phase-locked loop (PLL) automatic frequency locking, which is used to control the voltage and current of the circuit to be in phase [11, 12]. PLL can be divided into analog phase-locked loop (APLL) and digital phase-locked loop (DPLL). APLL uses analog circuits to control frequency and phase, while DPLL employs digital signal processing technology to achieve frequency and phase locking. APLL has a short locking time, but the design of the phase-locked circuit is complex, with poor noise resistance and low reliability [13–17]. Compared with APLL, DPLL has high accuracy and is not affected by temperature and voltage. The loop bandwidth and center frequency are programmable and adjustable, and when DPLL applied in digital systems, there is no need for A/D and D/A conversion. Therefore, APLL is gradually replaced by DPLL.

In MCR-WPT systems, DPLL is generally used to ensure that the system operates in a resonant state. To achieve DPLL in MCR-WPT systems, it is necessary to detect the phase relationship between the current and voltage of the primary coil in the system. The traditional phase difference detection method uses a comparison circuit to convert the current signal into a pulse width modulation (PWM) wave and inputs it together with the original voltage signal into the capture units of the programmable chips to obtain the phase difference between the current and voltage [18–20]. This approach is simple, but the capture units of the programmable chips have inherent sampling errors that cannot be overcome, making it difficult to meet high-precision requirements.

In order to overcome the insufficiency of traditional methods, in this paper a method for accurately detecting the phase difference of current and voltage signals in WPT systems using incomplete cross S transform (ICST) is proposed. The ability of ICST to accurately detect phase difference is specific to sinusoidal signals, so the proposed method requires corresponding low-pass filtering processing of the signals. The remainder of this paper is organized as follows. The foundation of this paper is introduced in Section 2. The phase difference detection method using ICST is reported in Section 3. The simulations made to verify the performance of the technique are documented in Section 4. Finally, the whole work is summarized in Section 5.

## 2. FOUNDATION

### 2.1. Typical Structure of WPT System

MCR-WPT system is composed of high frequency inverter circuit, compensation circuit, resonant coil, rectifierfilter circuit, and load. The input power is converted into high-frequency alternating current by inverter circuit, and the energy is transferred to the secondary side by resonant coil. The high-frequency AC power on the secondary side of the system is filtered and provided to the load. The equivalent circuit diagram of WPT system is shown in Figure 1.

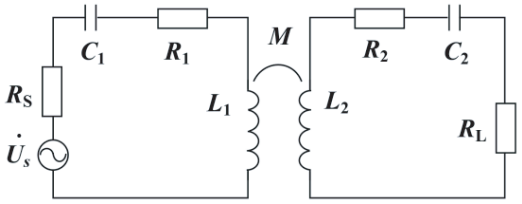


**Figure 1.** Equivalent circuit of the WPT system.

$\dot{U}_s$ is the AC voltage source of the primary side. $L_1$ and $L_2$ are the self-inductance of the primary side and secondary side of the coil, respectively. $C_1$ and $C_2$ are the compensation capacitors. $R_1$ and $R_2$ are the equivalent resistances of the primary and secondary side coils, respectively. $R_S$ is the internal resistor of the power source, and $R_L$ is the load resistance. $M$ is the mutual inductance between the primary side and the secondary side. According to Kirchhoff's voltage law (KVL), WPT system can be

expressed as [21, 22]:

$$\begin{cases} Z_1 = R_s + R_1 + j\omega L_1 + 1/(j\omega C_1) \\ Z_2 = R_L + R_2 + j\omega L_2 + 1/(j\omega C_2) \\ \dot{I}_1 = \dfrac{Z_2 \dot{U}_s}{Z_1 Z_2 + (\omega M)^2} \\ \dot{I}_2 = \dfrac{j\omega M \dot{U}_s}{Z_1 Z_2 + (\omega M)^2} \end{cases} \tag{1}$$

where $\dot{I}_1$ is the current at the coil transmitter, and $\dot{I}_2$ is the current at the coil receiver. $Z_1$ and $Z_2$ are the impedances at both ends.

### 2.2. Cross S Transform (CST)

Let $h(t) \in L^2(R)$, where $L^2(R)$ represents a square integrable space over a real number field, and the S transformation of $h(t)$ is defined as [23]:

$$S(\tau, f) = \int_{-\infty}^{\infty} h(t) \left\{ \frac{|f|}{\sqrt{2\pi}} \mathrm{e}^{-\frac{(t-\tau)^2 f^2}{2}} \right\} \mathrm{e}^{-\mathrm{j}2\pi f t} \mathrm{d}t \tag{2}$$

By using the convolution theorem, the S transform can be calculated by formula (3).

$$S(\tau, f) = \int_{-\infty}^{\infty} H(\alpha + f) \mathrm{e}^{-\frac{2\pi^2 \alpha^2}{f^2}} \mathrm{e}^{\mathrm{j}2\pi a \tau} \mathrm{d}\alpha \tag{3}$$

where $t$ is time; $f$ is frequency; and $\tau$ is the center of the Gaussian window. $H(\cdot)$ is the Fourier transform of $h(\cdot)$. Therefore, the fast calculation of S transformation can be achieved by utilizing fast Fourier transform (FFT). The above equation can be written as a discrete expression ($f \to n,\ \tau \to k$) for

$$\begin{cases} S[k, n] = \displaystyle\sum_{m=0}^{N-1} \left\{ H[m+n] \mathrm{e}^{-\frac{2\pi^2 m^2}{n^2}} \right\} \mathrm{e}^{\frac{\mathrm{j}2\pi m k}{N}}, \quad n \neq 0 \\ S[k, 0] = \dfrac{1}{N} \displaystyle\sum_{m=0}^{N-1} h(m), \quad n = 0 \end{cases} \tag{4}$$

where $N$ is the total length of signal sequence; $k$ and $n$ are time sampling points and frequency sampling points, respectively; $H[m]$ is the discrete Fourier transform of signal sequence $h(k)$.

The Cross S Transform (CST) of signals $u$ and $i$ is defined as

$$C_{ST}(\tau, f) = S_u(\tau, f) \{S_i(\tau, f)\}^* \tag{5}$$

where $S_u$ and $S_i$ are S transform results of $u$ and $i$, respectively; "$*$" means taking complex conjugate.

In order to investigate the phase difference extraction ability of CST, it is assumed that there is a constant phase difference between single frequency signals $u(t)$ and $i(t)$, as shown below:

$$\begin{cases} u(t) = \mathrm{e}^{\mathrm{j}2\pi\omega t} \\ i(t) = u(t)\mathrm{e}^{\mathrm{j}\theta} = \mathrm{e}^{\mathrm{j}2\pi\omega t + \mathrm{j}\theta} \end{cases} \tag{6}$$

where $\theta$ is the phase difference between the two signals. By using the Fourier transform of two signals and formula (2), the CST can be obtained as follows:

$$S_u(\tau, f) \{S_i(\tau, f)\}^* = \mathrm{e}^{-\frac{4\pi^2(\omega - f)^2}{f^2}} \mathrm{e}^{-\mathrm{j}\theta} \tag{7}$$

Obviously, the modulus of $C_{ST}(\tau, f)$ is the highest when $f = \omega$. Therefore, the phase extracted at the maximum amplitude of CST is the phase difference between $u(t)$ and $i(t)$. To adapt to digital system applications, the discrete expression of CST can be written as

$$C_{ST}[m, n] = S_u[m, n] \{S_i[m, n]\}^* \tag{8}$$

where $C_{ST}[m,n]$ is a complex matrix; the row coordinate $m$ is time; and the ordinate coordinate $n$ is frequency. Since the elements in the matrix are complex, the phase of the matrix elements obtained after the multiplication of $S_u[mn]$ and $\{S_i[mn]\}^*$ is the phase difference between them. Assuming that a certain element value of $C_{ST}[m,n]$ is $P[M,N]$, its phase reflects the phase difference of the $N$ frequency component at time $M$. Since the phase of S transformation is directly related to the original signal, the phase of $P[M,N]$ reflects the phase difference of the $N$ frequency component of the original signal $u$ and $i$ at time $M$.

## 3. THE PROPOSED TECHNIQUE

In this section, a phase difference detection method using ICST is proposed. Firstly, the necessary components of the frequency tracking control system are introduced. Then the implementation steps of the proposed method are explained in detail.

### 3.1. Frequency Tracking Control System

The system using the proposed method is shown in Figure 2. It is mainly composed of phase detector, pulse frequency modulation (PFM) waveform generator, and proportional-integral (PI) controller. Considering the unavoidable error of using PWM signal to calculate phase difference, the PWM voltage signal is converted into a sine signal through a low-pass filter. To eliminate phase errors caused by filter delay, the current signal is also passed through a filter with the same parameters. The delays caused by the two filters are almost the same, so it can be offset in subsequent calculations. Obviously, another advantage of doing so is that the high-frequency noise can be filtered out to a certain extent. The filters is a fourth-order active low-pass filter with a cutoff frequency of 100 kHz. By synchronous sampling, $I(t)$ and $U(t)$ are converted into discrete signal sequences $F_1[n]$ and $F_2[n]$ by using analog to digital converter (ADC) + data buffer. The phase difference ($\theta$) between $F_1[n]$ and $F_2[n]$ is obtained by the phase detector which is also the phase difference between $I_1$ and $U_s$. To achieve resonance in the

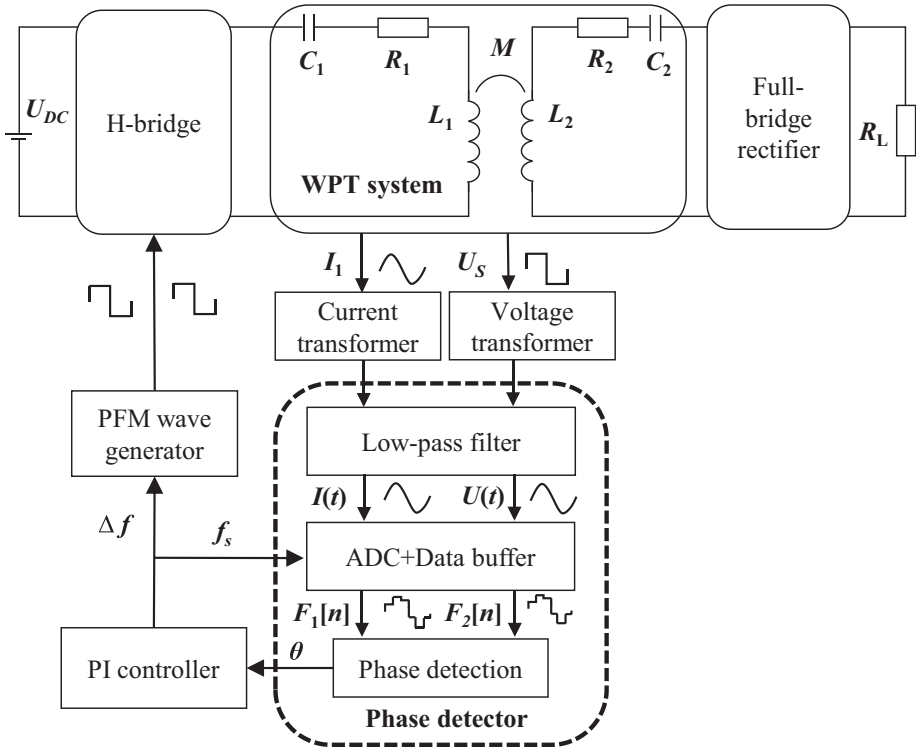


**Figure 2.** The schematic diagram of frequency tracking system.

WPT system, it is necessary to adjust $\Delta f$ through a PI controller to control the frequency of the PFM waveform generator. So that the current and voltage of the system gradually approach the same phase, that is, gradually reducing the phase difference to zero. At the same time, the sampling frequency $f_s$ of the ADC is controlled according to the frequency of the PFM, making it proportional to the system operating frequency, achieving synchronous sampling and providing the basic conditions for accurate detection of phase difference.

### 3.2. Phase Detector Using Incomplete CST (ICST)

Incomplete S transform (IST) only calculates the frequency points of interest, which improves the computational efficiency of S transform [24]. Introducing the calculation concept of IST, ICST only calculates the frequency points of interest, improving the computational efficiency of CST. The phase difference detection process using ICST is shown in Figure 3.

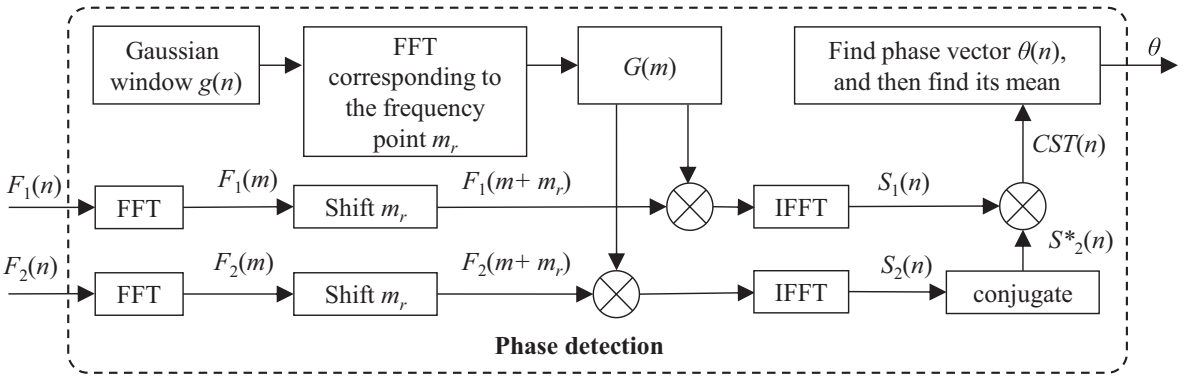


**Figure 3.** The operation diagram of phase detection.

In Figure 3, it is assumed that the main frequency of the obtained signal is $r$, and $m_r$ is the discrete frequency point corresponding to $r$. $g(n)$ is the discrete representation of the Gaussian window in formula (2). $G(m)$ is the Fourier transform of $g(n)$ corresponding to $m_r$. Combining Figure 2 and Figure 3, the phase detection method proposed in this paper can be described as the following steps:

Step 1: The low pass filter is used to eliminate the noise of the primary side voltage $U_s$ and the primary side current $I_1$ of the WPT system, and the waveform of $U_s$ is transformed into sine wave. The two outputs of the low-pass filter are $I(t)$ and $U(t)$.

Step 2: By synchronously sampling $I(t)$ and $U(t)$, discrete signals $I(n)$ and $U(n)$ are obtained. Then, they are transformed into finite length sequences $F_1[n]$ and $F_2[n]$ through ADC + data buffer.

Step 3: $F_1[m]$ and $F_2[m]$ are obtained by applying FFT operations to $F_1[n]$ and $F_2[n]$. Then $F_1[m]$ and $F_2[m]$ are shifted by $m_r$ to get $F_1[m+m_r]$ and $F_2[m+m_r]$.

Step 4: After multiplying G with $F_1[m+m_r]$ and $F_2[m+m_r]$, $S_1(n)$ and $S_2(n)$ are calculated using inverse fast Fourier transform (IFFT) operation.

Step 5: The product of $S_2^*(n)$ and $S_1(n)$, $C_{ST}(n)$, is the CST of the two signals, where $S_2^*(n)$ is obtained by conjugating $S_2(n)$.

Step 6: The phase vector $\theta(n)$ is obtained by extracting the phase of $C_{ST}(n)$. Then, the phase difference $\theta$ is obtained by averaging $\theta(n)$ from formula (9).

$$\theta = \frac{1}{b-a+1}\sum_{i=a}^{b}\theta(i), \quad a = \text{round}\left(\frac{N}{4}\right), \quad b = \text{round}\left(\frac{3N}{4}\right) \tag{9}$$

where $N$ is the total length of vector $\theta(n)$, and $round(\ )$ is an integral function.

To apply this method to frequency tracking of WPT system, it is necessary to preprocess the original signal. So the data buffer module is introduced, and the schematic diagram is shown in Figure 4, where $i$ is the index of sequence $F$, $l$ the length of the sequence, and $k$ the ratio of sampling frequency $f_s$ to

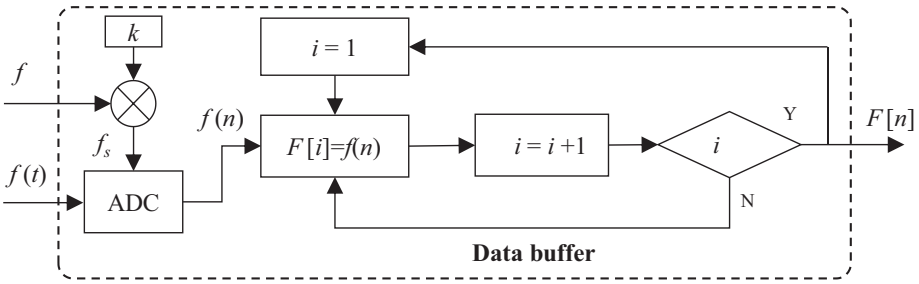


**Figure 4.** The control diagram of ADC + Data buffer.

system frequency $f$. The function of this module is to convert continuous signal to discrete signal by synchronous sampling, and the sampled data is temporarily stored in a buffer. When the data amount reaches the set length, it is output to the phase difference calculation unit.

## 4. EXPERIMENTS

In order to verify the feasibility of the proposed method for phase difference detection, experiments were carried out through MATLAB simulation [25]. These experiments take the working frequency $f = 100\,\text{kHz}$ as an example.

### 4.1. Experiment with Different Waveforms

In order to verify the accuracy of the proposed method for different waveforms, set sampling frequency $f_s = 1\,\text{MHz}$. Due to the possibility that data length may accumulate errors and affect the results, it is set to be short (128 points). As shown in Figure 5(a), the primary side voltage signal $u_s$ (pulsed square wave with duty cycle of 50%) and primary side current signal $u_i$ (sine wave) correspond to $U_s$ and $I_1$ respectively at the transmitter end of the WPT system. Set the amplitude of both signals as 1 V and the phase difference as 60°. The proposed method was used for phase difference detection, and the obtained phase vector $\theta(n)$ is shown in Figure 5(b).

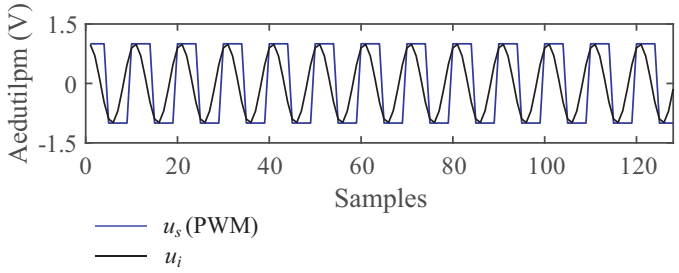


(a) Original signals

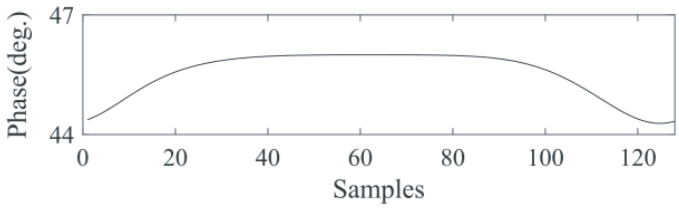


(b) Phase difference

**Figure 5.** Simulation results of pulse wave.

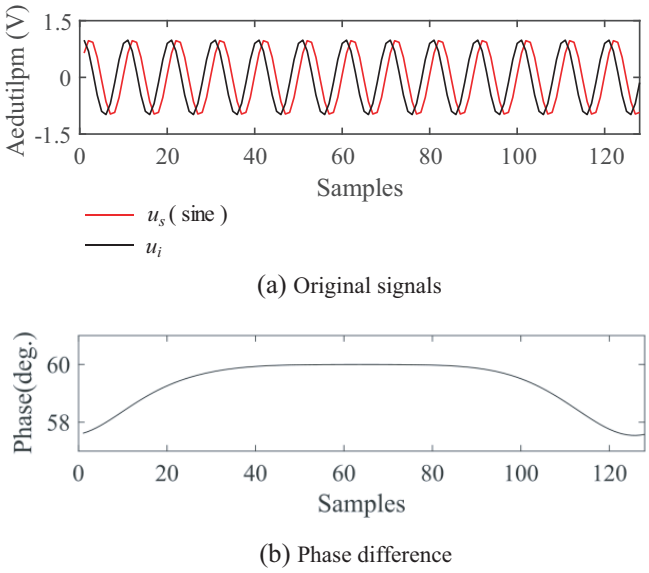


(a) Original signals

(b) Phase difference

**Figure 6.** Simulation results of sine wave.

Formula (9) is used to calculate the phase difference $\theta$, and the error is close to 14°. Therefore, for the detection of phase difference between pulsed square wave signal and sinusoidal signal, the proposed method has a large error. Due to the lag of zero crossing detection in sampling pulse square wave signals, the phase difference calculation error ranges from 0 to 360/k degrees. To eliminate this insurmountable error, it is necessary to convert the pulse square wave into a sine wave.

As shown in Figure 2, a low-pass filter is used to convert pulse square waves into sine waves, and the converted results are shown in Figure 6(a). The proposed method is then used to detect the phase difference, and the results are shown in Figure 6(b). It can be seen that after the pulse square wave signal is converted into a sinusoidal signal, the error calculated using this method is significantly reduced. The specific error analysis is shown in Table 1 and Table 2 of the experiment below.

**Table 1.** Phase error statistics under different noise conditions.

| SNR (dB) | Maximum | Error (degree) Minimum | Standard deviation |
|---|---|---|---|
| 10 | 6.6737 | −8.2880 | 2.5147 |
| 20 | 2.5697 | −2.4144 | 0.8040 |
| 40 | 0.2691 | −0.3288 | 0.0812 |
| 60 | 0.0250 | −0.0285 | 0.0084 |
| 80 | 0.0032 | −0.0025 | 8.0982e-04 |

**Table 2.** Statistics of phase difference errors under different data lengths.

| Length (point) | Maximum | Error (degree) Minimum | Standard deviation |
|---|---|---|---|
| 500 | 2.1387 | −2.3004 | 0.8113 |
| 1000 | 2.1131 | −1.7212 | 0.5672 |
| 2000 | 1.4638 | −1.3286 | 0.4047 |
| 10000 | 0.5740 | −0.6601 | 0.1756 |

### 4.2. Noise Resistance Test

To verify the anti-noise performance of the ICST, set a group of sinusoidal signals, $f_1(n)$ and $f_2(n)$, with phase difference of 0°; their amplitudes are 0.5 V and 1 V; and set the noise, SNR = 20 dB, as shown in Figure 7(a). Using the proposed method, the detected phase vector results are shown in Figure 7(b). Under the above parameter conditions, 1000 samples were randomly generated, and the error results of the phase difference detected using the proposed method are shown in Figure 7(c). The statistical values of the phase difference detection results obtained by changing the noise level using the same experimental method are shown in Table 1. As can be seen from Table 1, the larger the signal-to-noise ratio (SNR) is, the larger the maximum of phase difference error is, and the larger the standard deviation is. In the case of SNR > 40, the maximum phase difference error is less than 0.5°. The experimental results indicate that the proposed method is insensitive to noise.

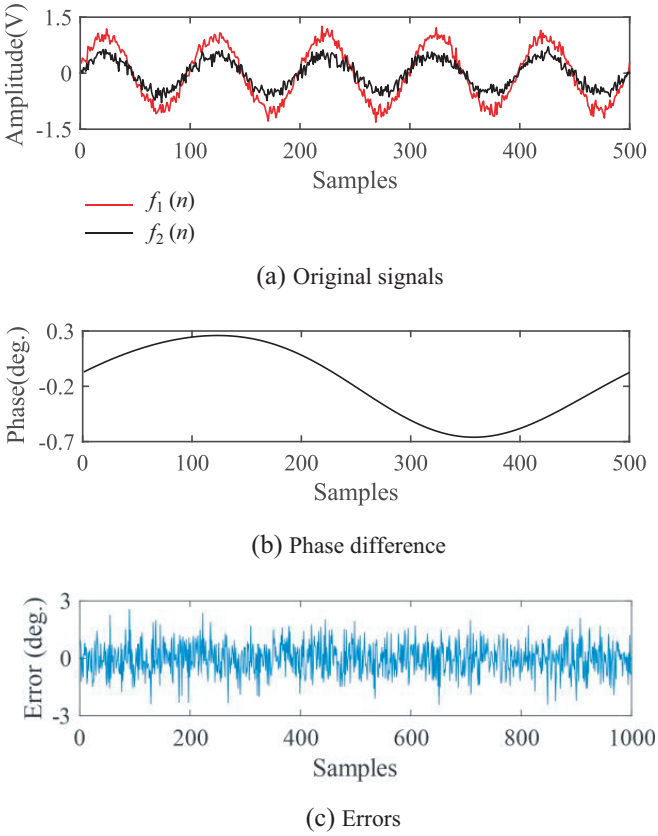


**Figure 7.** Simulation results under noise.

### 4.3. Filtering Experiment

To achieve waveform conversion function, a fourth-order active Butterworth low-pass filter with cutoff frequency 100 kHz has been designed. The sampling frequency used for verification is 10 MHz, and noise with an SNR of 20 dB is added. The original side current signal $u_i$ and voltage signal $u_s$ are shown in Figure 8(a). The phase difference between the two signals is 0°, and their amplitudes were 0.5 V and 1 V. The signals $u_i$ and $u_s$ are processed into $u_{if}$ and $u_{sf}$ after passing through low-pass filters, as shown in Figure 8(b). It can be seen that the two signals have been denoised, while the pulse square wave has been converted into a sine wave. It should be noted that the delay of the filter can cause phase error, and this error can be effectively eliminated by using two filters of the same model in this proposed method. Then the proposed method is used to detect the phase difference between the two signals $u_{if}$ and $u_{sf}$, and the error is less than 0.2°. The error caused by filter can be reduced by increasing

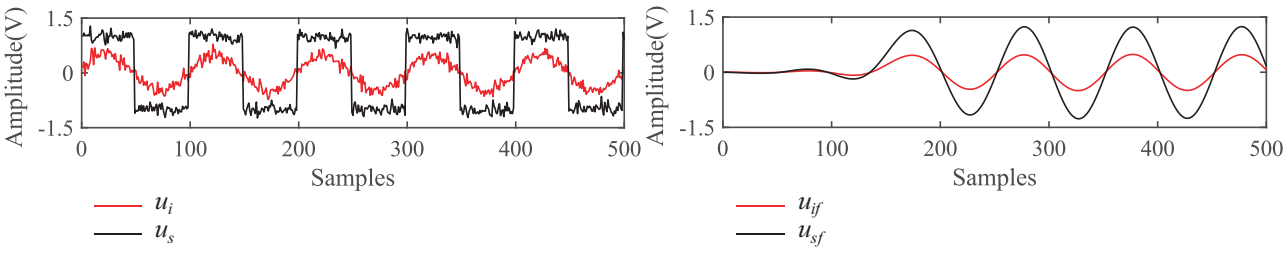


(a) Original signals (b) Results

**Figure 8.** Simulation results using the filter.

sampling frequency $f_s$. Therefore, analog filter rather than digital filter can be used to reduce errors, and calculations can also be reduced.

### 4.4. Discussion of Data Length and Sampling Frequency

To analyze the impact of using different data lengths for phase difference calculation on the error of the proposed method, experiments are conducted using different data lengths. The sampling frequency used for verification is 10 MHz, and the noise with an SNR of 20 dB is added. The experimental results are shown in Table 2. It can be seen that the maximum phase difference error decreases slowly with the increase of data length. Although the accuracy of detection can be improved by increasing the data length, exponentially increasing the computational cost is required. Therefore, the real-time performance of this method can be improved by appropriately reducing the length of the signal.

To verify the impact of data length and sampling frequency on errors, take the phase difference of 60° and SNR = 300. Sampling frequency ranges from $2 \times 1^5$ Hz to $10 \times 10^5$ Hz, the interval is $2 \times 10^4$ Hz. The data length ranges from 2 points to 50 points, with a 2 point interval. The phase difference detection experiment was conducted on the above signal using the proposed method, and the results are shown in Figure 9(a). It can be seen that the shorter the data length is, the greater the error is, which is consistent with the conclusion obtained above. In addition, when the data length is small, the higher the sampling frequency is, the greater the error is. This is because there are more data points in a signal cycle at a high sampling rate. However, when the data length is small, these data lengths cannot form a complete signal cycle, resulting in larger errors. From Figure 9(a), it can also be seen that as the sampling rate increases, the data length must be increased simultaneously to maintain the accuracy of the detection algorithm, in order to ensure that the data length can form at least one complete signal cycle. As shown in Figure 9(b), under synchronous sampling conditions, the optimal sampling frequency is $4 \times 10^5$ Hz, and the optimal data length is 4, which can achieve the comprehensive optimization of

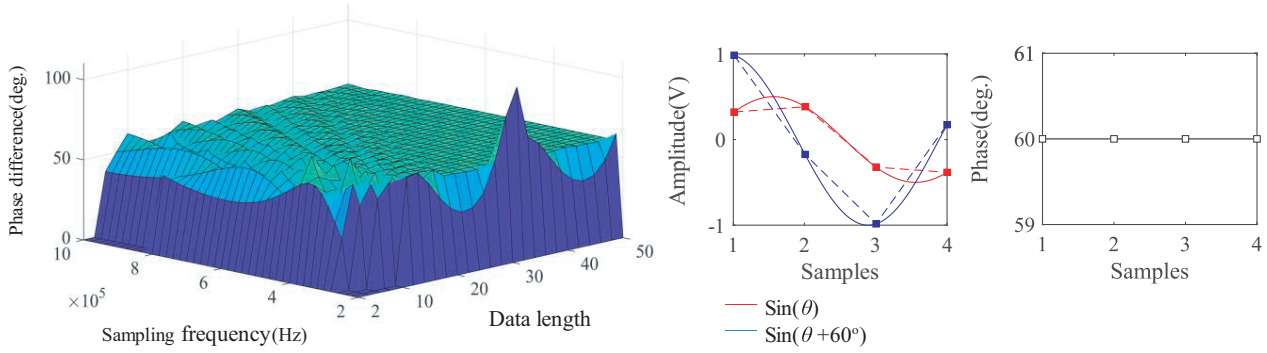


(a) Phases distribution (b) Results

**Figure 9.** Simulation results under various working conditions.

accuracy and real-time performance. Under this condition, the response time of the algorithm is about 1 signal cycle, which is 10 us. As the load and working environment change, the resonant frequency of the WPT system will change. Therefore, in order to maintain synchronous sampling, it is necessary to continuously change the sampling frequency, which can be adjusted according to the operating frequency generator of the control system.

## 5. CONCLUSION

It is a common method to realize frequency tracking of WPT system by using phase locked loop automatic frequency locking technology. In this paper, a new method of phase difference detection using ICST is proposed for phase detector in PLL. Compared with the traditional phase detector, this method has the advantages of high reliability and high precision. WPT system often works in complex and changeable environment. The simulation results have shown that the proposed phase detector has good noise resistance. The simplified computational performance of IST is inherited by ICST, and combined with synchronous sampling and using less data length, real-time application of the proposed algorithm can be achieved. Further research is needed to implement the proposed method using programmable chips and verify its adaptability in practical systems.

## ACKNOWLEDGMENT

This work was partially supported by Scientific Research Fund of Hunan Education Department of China (18A272) and the Natural Science Foundation of Hunan Province of China (2019JJ60055).

## REFERENCES

1. Kim, J., B. Clerckx, and P. D. Mitcheson, "Signal and system design for wireless power transfer: Prototype, experiment and validation," *IEEE Transactions on Wireless Communications*, Vol. 19, 7453–7469, 2019.
2. Yang, L., Y. Shi, M. Wang, and L. Ren, "Constant voltage charging and maximum efficiency tracking for WPT systems employing dual-side control scheme," *IEEE Journal of Emerging and Selected Topics in Power Electronics*, Vol. 10, 945–955, 2022.
3. Darvish, P., S. Mekhilef, and H. A. Illias, "A Novel S-S-LCLCC compensation for three-coil WPT to improve misalignment and energy efficiency stiffness of wireless charging system," *IEEE Transactions on Power Electronics*, Vol. 36, 1341–1355, 2021.
4. Shinohara, N., "Trends in wireless power transfer: WPT Technology for energy harvesting, mllimeter-wave/THz rectennas, MIMO-WPT, and advances in near-field WPT applications," *IEEE Microwave Magazine*, Vol. 22, 46–59, 2021.
5. Mahesh, A., B. Chokkalingam, and L. Mihet-Popa, "Inductive wireless power transfer charging for electric vehicles — A review," *IEEE Access*, Vol. 9, 137667–137713, 2021.
6. Liu, Y., "Overview of the development and application of radio energy transmission technology," *New Electrical Energy Technology*, Vol. 42, No. 2, 48–67, 2023.
7. Li, Z., P. Kong, L. Ren, X. Xiong, J. Li, W. Wu, and H. Liu, "Leakage magnetic field calculation and optimization of double inverse series coil structure of electric vehicle wireless charging systems," *Progress In Electromagnetics Research B*, Vol. 96, 213–233, 2022.
8. Li, J., Z. Han, and C. Guo, "Novel subarray partition algorithm for solving the problem of too low beam collection Efficiency caused by dividing a few subarrays," *Progress In Electromagnetics Research M*, Vol. 108, 223–235, 2022.
9. Zhang, X., "Frequency tracking control method for all digital radio energy transmission," *Journal of Electrical Machinery and Control*, Vol. 26, No. 2, 131–141, 2022.
10. Li, Z., W. Cheng, J. Yi, and J. Li, "Design and optimization of quasi-constant mutual inductance for asymmetric two-coil wireless power transfer system with lateral misalignments," *Progress In Electromagnetics Research M*, Vol. 69, 207–217, 2018.

11. Liu, Y., H. Feng, and X. Fan, "Adaptive fuzzy control for frequency tracking in magnetic coupled resonant radio energy transmission systems," *Electronic Devices*, Vol. 44, No. 6, 1385–1391, 2021.
12. Hou, F., "Design of enhanced digital phase locked loop for special operation equipment," *Technological Innovation and Application*, Vol. 13, No. 1, 112–115, 2023.
13. Khazraj, H., F. F. Da Silva, C. L. Bak, and S. Golestan, "Analysis and design of notch filter-based PLLs for grid-connected applications," *Electr. Power Syst. Res*, Vol. 147, 62–69, 2017.
14. Jayathurathnage, P. K., "Wireless power transfer based on novel physical concepts," *Nature Electronics*, Vol. 4, 707–716, 2021.
15. Liu, A., "Frequency composite control method for magnetic coupled resonant radio energy transmission systems," *Journal of Electrical Machinery and Control*, Vol. 24, No. 2, 63–71, 2020.
16. Gao, L., L. You, and X. Q. Wen, "Frequency tracking technology of magnetic coupling resonant wireless power transfer system," *Science Technology and Engineering*, Vol. 19, No. 8, 120, 2019.
17. Lee, C. K. and W. Zhong, "Effects of magnetic coupling of nonadjacent resonators on wireless power domino-resonator systems," *IEEE Transactions on Power Electronics*, Vol. 27, No. 4, 1905–1916, Apr. 2012.
18. Zhang, Y. and Z. Yan, "A high-power wireless charging system using LCL-N topology to achieve a compact and low-cost receiver," *IEEE Transactions on Power Electronics*, Vol. 35, No. 1, 131–137, May 2019.
19. Wen, D., Y. Zou, Z. Li, and J. Yi, "Mixed-modulation method for adjusting frequency and voltage in the WPT systems with misalignments and load variations," *Progress In Electromagnetics Research B*, Vol. 93, 111–129, 2021.
20. Xiao, F., L. Dong, L. Li, and X. Liao, "A frequency-fixed sogi-based PLL for single-phase grid connected converters," *IEEE Transactions on Power Electronics*, Vol. 32, 1713–1719, 2017.
21. Lee, C. K. and W. Zhong, "Effects of magnetic coupling of nonadjacent resonators on wireless power domino-resonator systems," *IEEE Transactions on Power Electronics*, Vol. 27, No. 4, 1905–1916, Apr. 2012.
22. Zhang, Y. and Z. Yan, "A high-power wireless charging system using LCL-N topology to achieve a compact and low-cost receiver," *IEEE Transactions on Power Electronics*, Vol. 35, No. 1, 131–137, May 2019.
23. Stockwell, R. G., "S-Transform analysis of gravity wave activity from a small scale network of airglow imagers," *London: The University of Western Ontario*, 1999.
24. Yi, J. and J. Peng, H. Tan, "Detection method of power quality disturbances using incomplete S-transform," *High Voltage Engineering*, Vol. 35, No. 10, 2562–2567, 2009.
25. Khan, S. M. and C. Bailey, "Efficient wireless power transfer (WPT) and field containment through chiral ordering of a four-tier wpt system," *IEEE USNC-URSI Radio Science Meeting (Joint with AP-S Symposium)*, Singapore, 2021.